

Multi-functional photonic spin Hall effect sensor controlled by phase transition

Jie Cheng(程杰), Rui-Zhao Li(李瑞昭), Cheng Cheng(程骋), Ya-Lin Zhang(张亚林), Sheng-Li Liu(刘胜利), and Peng Dong(董鹏)

Citation: Chin. Phys. B, 2024, 33 (**7**): 074203. DOI: 10.1088/1674-1056/ad3b85
Journal homepage: http://cpb.iphy.ac.cn; http://iopscience.iop.org/cpb

What follows is a list of articles you may be interested in

Engineered photonic spin Hall effect of Gaussian beam in antisymmetric parity-time metamaterials

Lu-Yao Liu(刘露遥), Zhen-Xiao Feng(冯振校), Dong-Mei Deng(邓冬梅), and Guang-Hui Wang(王光辉)
Chin. Phys. B, 2023, 32 (**9**): 094201. DOI: 10.1088/1674-1056/accb89

Asymmetrical photonic spin Hall effect based on dielectric metasurfaces

Guangzhou Geng(耿广州), Ruhao Pan(潘如豪), Wei Zhu(朱维), and Junjie Li(李俊杰)
Chin. Phys. B, 2022, 31 (**12**): 124207. DOI: 10.1088/1674-1056/ac754b

Enhancing terahertz photonic spin Hall effect via optical Tamm state and the sensing application

Jie Cheng(程杰), Jiahao Xu(徐家豪), Yinjie Xiang(项寅杰), Shengli Liu(刘胜利), Fengfeng Chi(迟逢逢), Bin Li(李斌), and Peng Dong(董鹏)
Chin. Phys. B, 2022, 31 (**12**): 124202. DOI: 10.1088/1674-1056/ac92d5

Photonic spin Hall effect and terahertz gas sensor via InSb-supported long-range surface plasmon resonance

Jie Cheng(程杰), Gaojun Wang(王高俊), Peng Dong(董鹏), Dapeng Liu(刘大鹏), Fengfeng Chi(迟逢逢), and Shengli Liu(刘胜利)
Chin. Phys. B, 2022, 31 (**1**): 014205. DOI: 10.1088/1674-1056/ac192a

Modulation and enhancement of photonic spin Hall effect with graphene in broadband regions

Peng Dong(董鹏), Gaojun Wang(王高俊), and Jie Cheng(程杰)
Chin. Phys. B, 2021, 30 (**3**): 034202. DOI: 10.1088/1674-1056/abccb2

Multi-functional photonic spin Hall effect sensor controlled by phase transition

Jie Cheng(程杰)[1,†], Rui-Zhao Li(李瑞昭)[1], Cheng Cheng(程骋)[2], Ya-Lin Zhang(张亚林)[1], Sheng-Li Liu(刘胜利)[1], and Peng Dong(董鹏)[3,‡]

[1] *School of Science, Jiangsu Province Engineering Research Center of Low Dimensional Physics and New Energy, Nanjing University of Posts and Telecommunications, Nanjing* 210023, *China*

[2] *College of Electronic and Optical Engineering, Nanjing University of Posts and Telecommunications, Nanjing* 210023, *China*

[3] *School of Electrical Engineering, Research Center of Intelligent Sensor and Network Engineering Technology of Jiangsu Province, Nanjing Vocational University of Industry Technology, Nanjing* 210023, *China*

(Received 1 February 2024; revised manuscript received 3 April 2024; accepted manuscript online 7 April 2024)

Photonic spin Hall effect (PSHE), as a novel physical effect in light–matter interaction, provides an effective metrological method for characterizing the tiny variation in refractive index (RI). In this work, we propose a multi-functional PSHE sensor based on VO_2, a material that can reveal the phase transition behavior. By applying thermal control, the mutual transformation into different phase states of VO_2 can be realized, which contributes to the flexible switching between multiple RI sensing tasks. When VO_2 is insulating, the ultrasensitive detection of glucose concentrations in human blood is achieved. When VO_2 is in a mixed phase, the structure can be designed to distinguish between the normal cells and cancer cells through no-label and real-time monitoring. When VO_2 is metallic, the proposed PSHE sensor can act as an RI indicator for gas analytes. Compared with other multi-functional sensing devices with the complex structures, our design consists of only one analyte and two VO_2 layers, which is very simple and elegant. Therefore, the proposed VO_2-based PSHE sensor has outstanding advantages such as small size, high sensitivity, no-label, and real-time detection, providing a new approach for investigating tunable multi-functional sensors.

Keywords: photonic spin Hall effect, multi-functional sensors, phase transition, sensing performance

PACS: 42.40.My, 42.25.–p, 41.20.Jb, 42.79.–e **DOI:** 10.1088/1674-1056/ad3b85

1. Introduction

As a fundamental optical property of a material, the accurate measurement of refractive index (RI) is of great importance for many chemical applications and researches.[1–3] Nowadays, due to the advantages of fast response and precise real-time detection, a variety of optical RI sensors have been developed, which are widely used to monitor the tiny change of the chemical constituents (e.g., 10^{-9} RIU, which corresponds to approximately 1 fmol/L of salt in water).[4–6] For example, Jian *et al*. demonstrated the highly sensitive cell concentration detection by exploiting the resonant optical tunneling effect (ROTE), with a desirable sensitivity of 19 μm/RIU.[7] It is reported that the nano-dot enhanced plasmonic biosensor can detect the fractional changes of the electrolyte concentration and glucose concentration in human blood.[8] However, most of the optical RI sensors can have a single function. Therefore, how to integrate multiple functions into one device and dynamically switch the functions according to different needs is an exciting but highly challenging issue.

The photonic spin Hall effect (PSHE) is a novel optical phenomenon that left- and right-handed circular polarization components of linearly polarized light split perpendicular to the incidence plane when the beam is reflected or transmitted at an interface.[9,10] The PSHE can be regarded as an optical analogy of the spin Hall effect (SHE) in electronic systems, in which spin electrons and an electric potential gradient are replaced by the spin photons and RI gradient, respectively.[11,12] The intrinsic mechanism of PSHE is related to the interaction between the photon-spin (polarization) and the trajectory (extrinsic orbital angular momentum).[12] Recently, the PSHE in photonic crystals and compound grating waveguide structures were great enhanced.[13–15] The spin shifts generated by the PSHE are very sensitive to the RI changes, therefore, it will provide a new platform for precision metrology and highly sensitive RI sensing.[16–21] Very recently, multi-functional sensing devices based on the PSHE have been vigorously developed, which can make full use of material properties and realize the multiple sensing detections. Sui *et al*. proposed a highly sensitive Janus sensor to achieve the multi-tasking of thickness and RI detections on two different scales.[22] The number of graphene layers is exactly identified on the forward scale; while on the backward scale of RI detection, different kinds of waterborne bacteria can be discriminated with high precision. Then the detection of multiple physical quantities (RI, thickness, and incidence angle) is

†Corresponding author. E-mail: chengj@njupt.edu.cn
‡Corresponding author. E-mail: 2021101298@niit.edu.cn

© 2024 Chinese Physical Society and IOP Publishing Ltd

also reported in another Janus sensor based on the PSHE.[23] As a consequence, the PSHE offers an effective way to realize multi-functional detections, and has broad prospects in the field of multi-scenario applications. Note that the above-mentioned Janus feature is derived from the complex multi-layer structure with the asymmetric arrangement of different dielectrics, which may be inconvenient to manufacture devices. Therefore, the design of multi-functional PSHE sensor with both the simple structure and excellent sensing performance is highly desirable.

In this work, we present a novel method to construct the multi-functional PSHE sensor by taking advantage of vanadium dioxide (VO_2), a material that can reveal the phase transition behavior. This sensor that we design is composed of only two VO_2 layers and one analyte layer, which is very simple and elegant. VO_2 is a temperature-dependent material, and it undergoes a phase transition from an insulating monoclinic phase to a metallic tetragonal phase at around 68°, which leads its dielectric permittivity and RI to significantly change.[24–26] By using this property, we can switch multi-functional sensing detections at different temperatures through thermal control. The PSHE sensor can achieve three different functions depending on the phase state of VO_2: when it is in the insulating state (at low temperature), it can detect the glucose concentration in the human blood; when it is in a mixed phase of insulating state and metallic state (at moderate temperature), it can achieve precise distinction between normal cells and cancer cells; when it is in the metallic state (at high temperature), it can be used as a gas sensor with the superior sensing performance.

2. Theory and model

The proposed PSHE sensor is shown in Fig. 1(a), which consists of two VO_2 layers and one analyte layer. Here, the VO_2 layers are regarded as having a semi-infinite width. The two VO_2 layers are controlled by the thermal control, and the sensing medium with the RI of n can be injected into the cavity (with the thickness of 1834 nm) between two VO_2 layers. The optical properties of VO_2 can be described by the complex permittivity, and the phenomenological model based on two lossy Lorentz oscillators is used to obtain the dielectric permittivity of both insulating and metallic phases:[27]

$$\varepsilon_{\text{ins,met}}\{E\} = \varepsilon_\infty + \sum_n \frac{A_n}{(E_n^2 - E^2) - \mathrm{i}EB_n}, \tag{1}$$

where $\varepsilon_{\text{ins,met}}$ is the complex permittivity in insulating (metallic) state as a function of photon energy E, ε_∞ is the high-frequency dielectric permittivity, A_n is the n-th oscillator amplitude, E_n is the n-th oscillator energy, and B_n is the n-th oscillator damping. The above-mentioned parameters for both insulating state and metallic state are given in Ref. [27]. The phase transition of VO_2 occurs gradually, and therefore, the dielectric permittivity ε_{mix} for a mixed phase of insulating state and metallic state can be expressed as[27]

$$\varepsilon_{\text{mix}}(T) = f(T)\,\varepsilon_{\text{ins}} + [1 - f(T)]\varepsilon_{\text{met}}, \tag{2}$$

$$f(T) = \frac{1}{\exp\left(\frac{T - T_{\text{t}}}{WT_{\text{t}}}\right) + 1}, \tag{3}$$

where $f(T)$ is a temperature-dependent function governing the distribution of insulating state and metallic state. $T_{\text{t}} = 333$ K is the transition temperature, and $W = 0.01$.

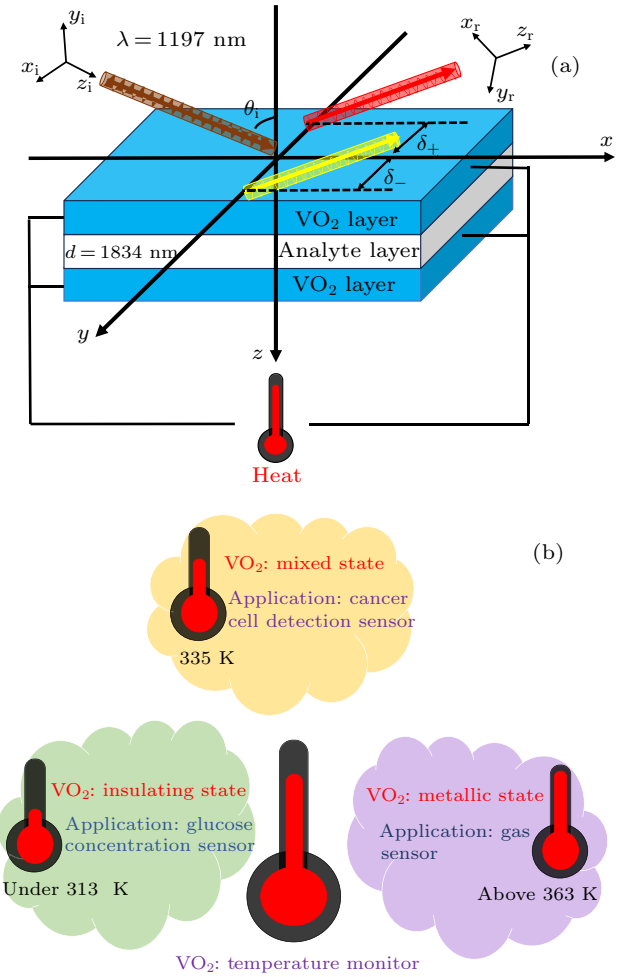


Fig. 1. (a) Schematic diagram of proposed sensor and corresponding PSHE. (b) Multiple RI sensing tasks by tuning temperature of VO_2 layers.

The PSHE is usually described by a general propagation model using the angle spectrum theory. We consider an incident Gaussian beam whose angle spectrum can be written as[28]

$$\tilde{E}_{\text{i}} = \frac{w_0}{\sqrt{2\pi}} \exp\left[-\frac{(k_x^2 + k_y^2)w_0^2}{4}\right], \tag{4}$$

where w_0 is the beam waist: $w_0 = 30\lambda$ ($\lambda = 1197$ nm). The relation between the angle spectrum of the reflected beam and the angle spectrum of the incident beam can be described as[28]

$$\begin{bmatrix} \tilde{E}_{\text{r}}^{\text{H}} \\ \tilde{E}_{\text{r}}^{\text{V}} \end{bmatrix} = \begin{bmatrix} r_{\text{p}} & \frac{k_{\text{ry}}\cot\theta_{\text{i}}(r_{\text{p}} + r_{\text{s}})}{k_0} \\ -\frac{k_{\text{ry}}\cot\theta_{\text{i}}(r_{\text{p}} + r_{\text{s}})}{k_0} & r_{\text{s}} \end{bmatrix} \begin{bmatrix} \tilde{E}_{\text{i}}^{\text{H}} \\ \tilde{E}_{\text{i}}^{\text{V}} \end{bmatrix}, \tag{5}$$

in which $\tilde{E}_{\rm r}^{\rm H,V}$ and $\tilde{E}_{\rm i}^{\rm H,V}$ are the horizontal component (H) and vertical component (V) of the angle spectrum for the reflected beam and incident beam, respectively, k_0 is the wave number in free space, $r_{\rm s}$ and $r_{\rm p}$ are the Fresnel reflection coefficients of s and p waves, and can be calculated by the transfer matrix method[29]

$$M = T_{01}P_1T_{12}P_2\cdots P_{m-2}T_{m-2,m-1}P_{m-1}T_{m-1,m}, \tag{6}$$

where

$$T_{m-1,m} = \frac{1}{t_{m-1,m}}\begin{bmatrix} 1 & r_{m-1,m} \\ r_{m-1,m} & 1 \end{bmatrix} \tag{7}$$

is the transformation matrix from layer $(m-1)$ to layer m, and

$$P_m = \begin{bmatrix} \exp(-{\rm i}k_{mz}d_m) & 0 \\ 0 & \exp({\rm i}k_{mz}d_m) \end{bmatrix} \tag{8}$$

is the transmission matrix for layer m. Here, d_m is the thickness of layer m. $r_{m-1,m}$ and $t_{m-1,m}$ are reflection coefficient and transmission coefficient from layer $(m-1)$ to layer m, respectively. The Fresnel reflection coefficients can be given by the elements of transfer matrix

$$r_{\rm p,s} = \frac{M_{21}}{M_{11}}. \tag{9}$$

Then the spin shift of the reflected light can be defined as[30]

$$\delta_{\pm}^{\rm H} = \mp\frac{k_0w_0^2{\rm Re}(1+r_{\rm s}/r_{\rm p}){\rm cot}\theta_{\rm i}}{k_0^2w_0^2+\left|\frac{\partial \ln r_{\rm p}}{\partial\theta_{\rm i}}\right|^2+|(1+r_{\rm s}/r_{\rm p}){\rm cot}\theta_{\rm i}|^2}, \tag{10}$$

$$\delta_{\pm}^{\rm V} = \mp\frac{k_0w_0^2{\rm Re}(1+r_{\rm p}/r_{\rm s}){\rm cot}\theta_{\rm i}}{k_0^2w_0^2+\left|\frac{\partial \ln r_{\rm s}}{\partial\theta_{\rm i}}\right|^2+|(1+r_{\rm p}/r_{\rm s}){\rm cot}\theta_{\rm i}|^2}. \tag{11}$$

Obviously, the dielectric permittivity of VO_2 can be flexibly tuned by external thermal control, therefore, so Fresnel reflection coefficients and then the spin shifts of PSHE will change accordingly. In the different temperature ranges, the spin shifts will differ significantly. As clearly indicated in Fig. 1(b), this property makes it possible to achieve the multi-functional sensing by switching the phase states (i.e., the insulating, metallic, or mixed state) of VO_2.

For the PSHE-based RI sensors, the sensing performance can be evaluated by the intensity sensitivity and angle sensitivity. According to the intensity-based shift sensing mechanism, the intensity sensitivity of PSHE sensor can be defined as $S_\delta = \Delta\delta/\Delta n$,[31] where $\Delta\delta$ is the difference in the peak/valley of spin shift caused by an RI change of analyte sample, Δn. Similarly, $S_\theta = \Delta\theta/\Delta n$[32] is used to describe the angle sensitivity, in which $\Delta\theta$ is the variation of incident angle, corresponding to the peak/valley of spin shift. In the next section, we will focus on the detailed multi-functional sensing by this VO_2-based PSHE sensor, and the related sensing performance is systematically discussed.

3. Simulation results and analyses

The essential material of this novel PSHE sensor is VO_2, and the temperature can be a tunable parameter to control the permittivity of VO_2 (as indicated in Eqs. (1)–(3)). The relationship between the complex RI and temperature of VO_2 is shown in Fig. 2(a), which clearly displays the phase transition process of VO_2 from an insulating state (under 313 K) to a metallic state (above 363 K). More precisely, the real part of RI for VO_2 decreases from 2.49 to 2.05 with the increase of temperature, while its imaginary part increases from 0.36 to 0.87. Within the temperature region of 313 K–363 K, it is the so-called mixed phase of VO_2 (i.e., a superposition of the insulating and metallic states). This obvious change of RI can effectively control the PSHE of VO_2-based sensor, as shown in Fig. 2(b). Thereinto, the RI of the analyte layer is set to be 1.3, and we plot the spin shift $\delta_+^{\rm H}$ of PSHE sensor under different temperatures. Under the conditions of 313 K and 323 K, the spin shift exhibits an obvious peak around the incident angle of 21°. By increasing the temperature, the magnitude of peak gradually decreases, and then a deep valley is clearly seen at a lower incident angle of about 14° under the conditions of 343 K and 353 K. These tunable optical properties and the high sensitivity to temperature of VO_2 make it desirable to achieve the multi-functional sensing.

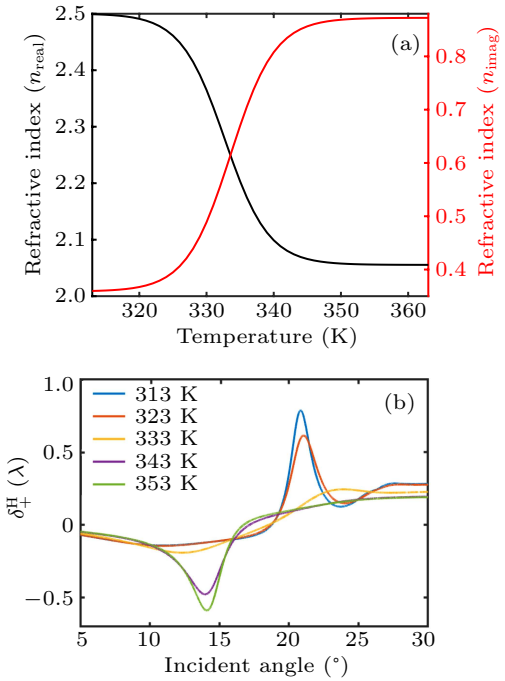


Fig. 2. (a) Relationship between the complex refractive index of VO_2 and temperature, and (b) plots of spin shift $\delta_+^{\rm H}$ *versus* incident angle of VO_2-based PSHE sensor under different temperatures.

In order to switch flexibly between different functions and further improve the sensing performance, it is necessary to explore the RI-sensitive values of this PSHE sensor under different temperatures, which correspond to the three different states of VO_2. As shown in Fig. 3, when VO_2 is in the insulating state at low temperature (under 313 K), the absolute value

of spin shift $|\delta_+^{\mathrm{H}}|$ for reflected beam can reach 7.31λ–7.61λ by fixing the incident angle of 24.10°, and corresponding sensitive RI value of the analyte layer is around 1.617. For the case of 335 K (the mixed state of VO_2), the related absolute value of spin shift undergoes a significant variation (6.99λ–9.3λ) at 17.91° by a tiny RI change of 1.399–1.400. When the temperature is above 363 K, VO_2 becomes a metallic state. At a fixed angle of 11.57°, the absolute value of spin shift varies from 8.35λ to 9.03λ with the RI of analyte layer increase from 1.000 to 1.002. Based on the above discussion, this VO_2-based PSHE sensor is expected to realize the multi-functional sensing by taking advantage of the obvious differences in sensitive RI values under different temperatures.

Firstly, we discuss the detection of glucose concentrations in the human blood by using this multi-functional PSHE sensor, when VO_2 is in the insulating state (at low temperature below 313 K). As displayed in Fig. 4(a), the spin shift δ_+^{H} of PSHE is very sensitive to the RI change of analyte layer, and its sign transforms from negative to positive around the incident angle of 24.4°, as the RI increases from 1.60 to 1.64. Fortunately, the RI of glucose solution in human blood is within this RI-sensitive region, and therefore, the PSHE sensor provides the opportunity for detecting the glucose concentrations when VO_2 is in an insulating state.

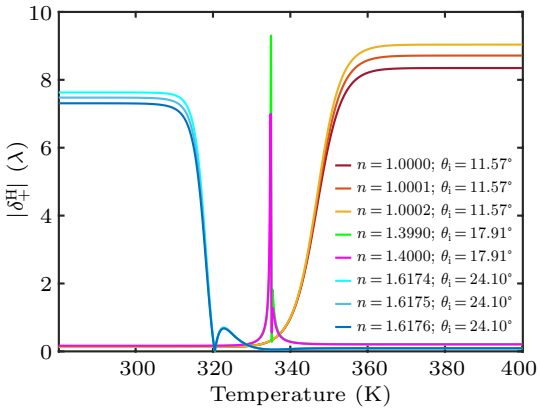


Fig. 3. Illustration of the RI sensitive value for this VO_2-based multi-functional PSHE sensor under different temperatures for various values of n and θ_i.

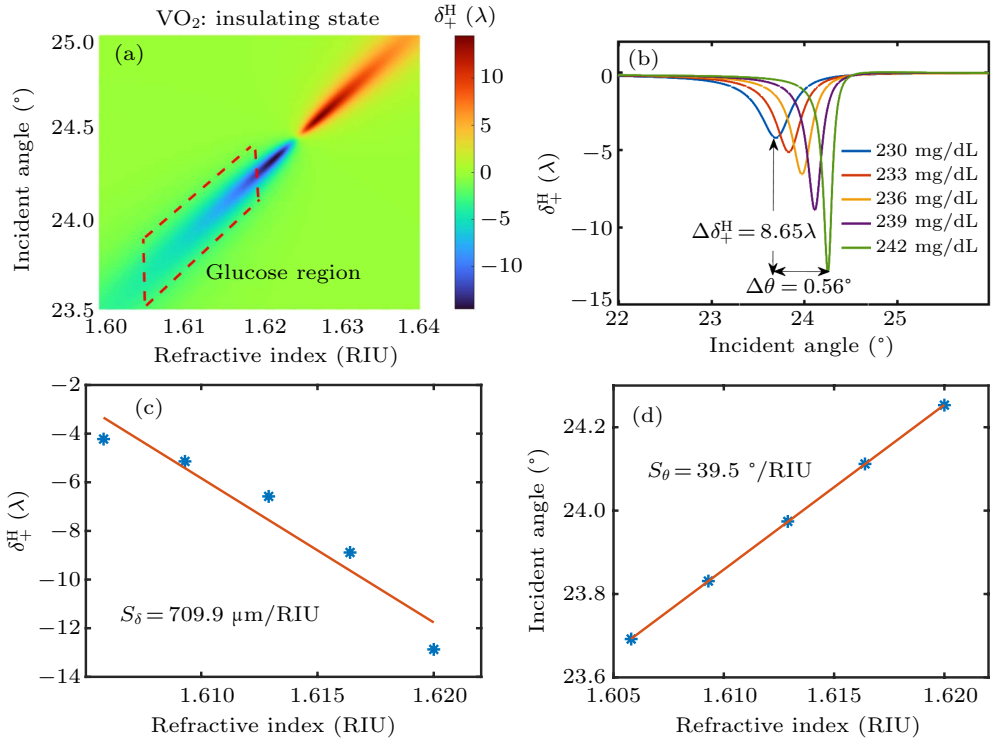


Fig. 4. Detection of glucose concentrations in human blood when VO_2 is in insulating state. (a) Spin shift δ_+^{H} as a function of incident angle and RI of analyte layer. (b) Dependence of spin shift on glucose concentration. (c)–(d) Description of the intensity sensitivity and angle sensitivity for detecting the glucose concentrations.

Table 1. Values of RI of glucose solution in human blood,[33] and the intensity/angle sensitivity for detecting glucose concentrations.

Sample	Concentration (mg/dL)	RI value (RIU)	$\delta_+^{\mathrm{H}}(\lambda)$	θ (°)	S_δ (μm/RIU)	S_θ (°/RIU)
Glucose ($k = 10$)	230	1.6058	–4.22	23.69	709.9	39.5
	233	1.6093	–5.14	23.83		
	236	1.6129	–6.58	23.97		
	239	1.6164	–8.89	24.11		
	242	1.6200	–12.87	24.25		

For the glucose solution in human blood, there is a linear relationship between the RI and glucose concentration,[33] which can be expresses as

$$n_{\text{Glucose}} = 0.0001189Ck + 1.33230545, \tag{12}$$

where C is the glucose concentration in units mg/dL, and k represents the glucose concentration factor. Here, we adopt the glucose concentration ranging from 230 mg/dL to 242 mg/dL, and the values of RI for these different concentrations are summarized in Table 1. When the glucose concentration increases, the values of RI in a range from 1.6058 to 1.6200, and this RI region of glucose solution is also labeled in Fig. 4(a). Figure 4(b) exhibits the spin shift *versus* incident angle under these different glucose concentrations, and we find that the spectrum of spin shift presents a relative displacement towards a larger angle as the glucose concentration increases, accompanied by an obviously deeper valley. When the glucose concentration in human blood equals 230 mg/dL, the maximal spin shift of -4.22λ is obtained at an incident angle of 23.69°; while for the condition of 242 mg/dL, they are -12.87λ and 24.25°, respectively. Therefore, the maximal spin shift undergoes the difference $\Delta\delta_+^{\text{H}}$ of 8.65λ, with the $\Delta\theta$ of 0.56°. The detailed data of maximal spin shift and corresponding incident angle for these different glucose concentrations are given in Figs. 4(c) and 4(d), which basically display a linear relation. By calculating the slope of linear-fitting curve, the intensity sensitivity and angle sensitivity can reach 709.9 μm/RIU and 39.5°, respectively. Note that this intensity sensitivity is much larger than the intensity sensitivities of some other classical glucose sensors (seen in Table 2).[33–38] Therefore, our proposed VO_2-based PSHE sensor presents the superior sensing performance for detecting the glucose concentration in human blood, when VO_2 is in the insulating state.

Table 2. Comparisons of our PSHE sensor with other classical glucose sensors.

Working principle/materials	Sensitivity (μm/RIU)	Reference
SPR	1.6	[34]
Resonance cavities	10	[35]
Multimode interference	1.5	[36]
Tricore photonic crystal fibre	23.3	[37]
Infrared metamaterial	2.7	[38]
Slot waveguide-based SOI ring resonator	0.4	[33]
PSHE	709.9	this work

Secondly, when VO_2 is in a mixed state (at a temperature of 335 K), the VO_2-based PSHE can be introduced for rapidly detecting different types of cancer cell, such as adrenal glands cancer (PC-12) and two types of breast cancers (MCF-7 and MDA-MB-231). Compared with the normal cells, cancer cells generally exhibit the larger RI because their larger nuclei contain more chromatin, as clearly observed in Table 3. The RI values of normal cells are in a range of 1.38–1.39, and those of the corresponding cancer cells are in a range of about 1.39–1.40. For instance, the MCF-7 breast normal cell has an RI value of 1.387, while the corresponding cancer cell possesses an RI value of 1.401. As shown in Fig. 5(a), the region framed with black dashed line is the RI region of normal cells, and the region of cancer cells is boxed with the red line. Note that these subtle differences in RI will result in the great variations of PSHE. The values of spin shift δ_+^{H} for different types of normal cells and cancer cells are presented in Fig. 5(b).

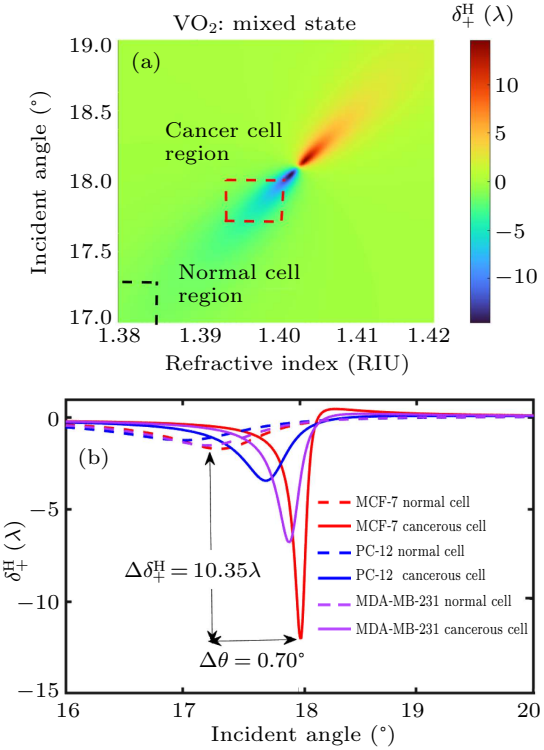


Fig. 5. Distinction between cancer cells and normal cells when VO_2 is in a mixed state. (a) Spin shift δ_+^{H} *versus* incident angle and RI of analyte layer. (b) Variations of spin shift with incident angle for different normal cells and cancer cells.

The signs of spin shifts for all cells are negative in an angle range of 16.0°–18.1° with a deepest valley appearing at the characteristic incident angle. The valley of spin shift for cancer cells is even deeper than that for normal cells, meanwhile, the incident angle corresponding to valley shifts toward a higher angle. Here, the magnitude of spin shift valley can provide a simple and rapid method for distinguishing the normal cells and cancer cells. More specifically, when the absolute value of valley is larger than 2λ, the analyte cells can be identified as cancer ones. Taking the MCF-7 normal cells and cancer cells for example, we evaluate the sensing performance of this VO_2-based PSHE sensor. For MCF-7 normal cells, the deepest valley (-1.69λ) of spin shift appears at an incident angle of 17.31°, while for cancer cells the deepest valley (-12.04λ) occurs at an incident angle of 18.01°. There exists a difference $\Delta\delta_+^{\text{H}}$ of 10.35λ in spin shift with the angle change $\Delta\theta$ of 0.70°. Combined with the RI difference Δn

of 0.014 RIU, the intensity (angle) sensitivity for distinguishing the MCF-7 normal cells and cancer cells can be calculated to be 884.9 μm/RIU (50 °/RIU). Similarly, the intensity and angle sensitivity values of PC-12 and MDA-MB-231 cells are also listed in Table 3. It is straightforward to observe that the angle sensitivities for these three cell types show no difference, while the intensity sensitivity reaches up to 884.9 μm/RIU for distinguishing the MCF-7 normal cells and cancer cells. According to previous report, the wavelength sensitivity of an optimized bowl-shaped mono-core SPR sensor is 180.7 μm/RIU for the similar detection of MCF-7 breast cancer.[39] Consequently, when VO_2 is in a mixed state, the proposed multifunctional PSHE sensor exhibits the prominent sensing performance for cancer detection with no-lable, and the intensity sensitivity is about 50 times greater than that of SPR sensor.

Finally, the VO_2-based PSHE sensor can be used to analyze the gas analytes with different values of RI, when VO_2 is in a metallic state (at a temperature above 363 K). The spin shift δ_+^{H} as a function of incident angle and RI of analyte layer is shown in Fig. 6(a). Obviously, by increasing the RI of analyte layer from 1 to 1.004, the sign of spin shifts changes from negative to positive at an incident angle of 11.7°. Here, we adopt the gas analytes with the values of RI in a range of 1–1.0012, and this RI region is also marked with the red lines (see Fig. 6(a)). As clearly shown in Fig. 6(b), the spin shift is very sensitive to the RI change of gas analytes. With the increase of RI of gas, an evident shift toward higher incident angle is observed in the spectrum of spin shift, accompanied by the deeper valley. For instance, when the RI of gas equals 1, there is a valley of -8.30λ in spin shift at an incident angle of 11.57°. While the spin shift is significantly enhanced to -14.21λ, as the gas RI increases to 1.0012. To quantitatively estimate the sensing performance of this VO_2-based PSHE sensor for the gas analysis, the valley value of spin shift and the corresponding incident angle as a function of gas RI are displayed in Figs. 6(c) and 6(d). Then, the intensity sensitivity of 601.6 μm/RIU and angle sensitivity of 48.7°/RIU are readily obtained by the linear fitting method.

Table 3. Values of RI for MCF-7, PC-12, MDA-MB-231 cancer/normal cells,[39] and intensity/angle sensitivity of VO_2-based PSHE sensor for cancer detection.

Cell Name	Cell types	RI value (RIU)	δ_+^{H} (λ)	θ (°)	S_δ (μm/RIU)	S_θ (°/RIU)
MCF-7	normal cell	1.387	–1.69	17.31	884.9	50
	breast cancer	1.401	–12.04	18.01		
PC-12	normal cell	1.381	–1.22	17.01	189.9	50
	Adrenal glands cancer	1.395	–3.43	17.71		
MDA-MB-231	normal cell	1.385	–1.50	17.21	452.3	50
	breast cancer	1.399	–6.79	17.91		

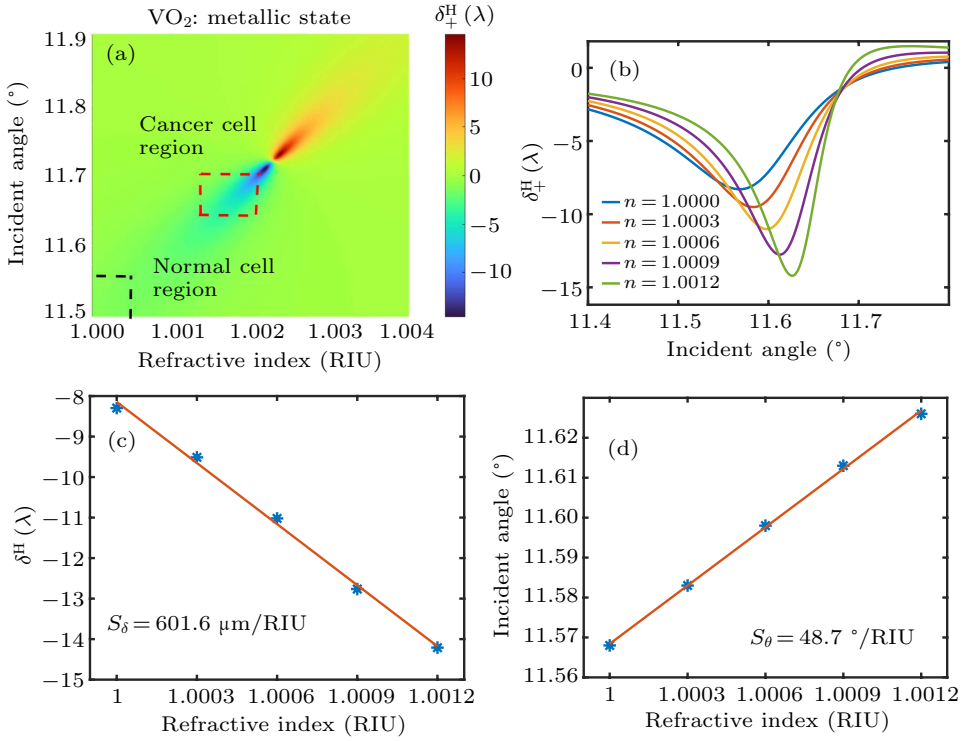


Fig. 6. Gas sensor when VO_2 is in a metallic state. (a) Spin shift δ_+^{H} as a function of incident angle and RI of gas analytes. (b) Variation of spin shift with the value of RI of gas. Variation of (c) intensity sensitivity and (d) incident angle with refractive index.

The above research indicates that only by manipulating the temperature of VO_2, the proposed PSHE sensor in this work exhibits the multiple RI sensitive ranges, which supports the flexible transformations in different sensing tasks, including the sensitive detection of glucose concentration in human blood, the distinction between cancer cells and normal cells with no-label, and the real-time monitoring of gas analytes.

4. Conclusions

In this work, we proposed a multi-functional PSHE sensor based on VO_2, a phase transition material that can switch between the insulating, mixed, and metallic states under different temperatures. Compared with the results reported previously, the VO_2-based sensor in this work is simple and elegant, which consists of only three layers: two VO_2 layers and an analyte layer. The proposed PSHE sensor can achieve three different functions depending on the phase state of VO_2: when it is in the insulating state, the sensor can detect the glucose concentration in human blood; when it is in a mixed state, different types of normal cells and cancer cells can be sensitively distinguished with no label; when it is in the metallic state, this PSHE sensor can act as a gas RI analyzer. The proposed multi-functional PSHE sensor has the advantages of high sensitivity, no-label, and real-time monitoring, which can be used in various application scenarios, and can flexibly switch the multiple sensing tasks by tuning the temperatures.

This work is only a theoretical study, and the experimental design is also anticipated. The structure of this sensor is simple and easy to achieve, and the temperature range (313 K–363 K) is not the extreme condition. Therefore, our proposed sensor will be feasible in the experiment. Taking the detections of glucose concentrations, cancer cells, and gas analytes for example, we confirm the multi-functional sensing of this sensor. In fact, our proposed sensor can also detect other analytes. When we detect different analytes, the operating wavelength of incident light can be accordingly changed (e.g., the terahertz band) to enhance the sensitivity and obtain the superior sensing performance.

Acknowledgements

Project supported by the National Natural Science Foundation of China (Grant No. NSFC 12175107), the Natural Science Foundation of Nanjing Vocational University of Industry Technology, China (Grant No. YK22-02-08), the Qing Lan Project of Jiangsu Province, China; the Postgraduate Research & Practice Innovation Program of Jiangsu Province, China (Grant No.KYCX23_0964), the Natural Science Foundation of Jiangsu Province, China (Grant No. BK20230347), and the Fund from the Research Center of Industrial Perception and Intelligent Manufacturing Equipment Engineering of Jiangsu Province, China (Grant No. ZK21-05-09).

References

[1] Kazanskiy N L, Khonina S N and Butt M A 2020 *Physica E* **117** 113798
[2] Uniyal A, Srivastava G, Pal A, Taya S and Muduli A 2023 *Plasmonics* **18** 735
[3] Zanchetta G, Lanfranco R, Giavazzi F, Bellini T and Buscaglia M 2017 *Nanophotonics* **6** 627
[4] Khalil M A, Yong W H, Hoque A, Isam M S, Chiong L Y, Leei C C, Albadran S, Soliman M S and Islam M T 2023 *Eng. Sci. Technol.* **48** 101582
[5] Ansari G, Pal A, Srivastava A K and Verma G 2023 *Opt. Laser Technol.* **164** 109495
[6] Eddin F B K, Fen Y W, Liew J Y C and Daniyal W M E M M 2022 *Biosensors* **12** 1124
[7] Jian A J, Zou L, Bai G, Duan Q Q, Zhang Y X, Zhang Q W, Sang S B and Zhang X M 2019 *J. Lightwave Technol.* **37** 2800
[8] Hassan M F, Sagor R H, Amin M R, Islam M R and Alam M S 2021 *IEEE Sens. J.* **21** 17749
[9] Zhao Y, Yang C X, Zhu J X, Lin F, Fang Z Y and Zhu X 2020 *Chin. Phys. B* **29** 067301
[10] Yu X T, Wang X, Li Z, Zhao L T, Zhou F F, Qu J L and Song J 2021 *Nanophotonics* **10** 3031
[11] Onoda M, Murakami S and Nagaosa N 2004 *Phys. Rev. Lett.* **9** 083901
[12] Lodahl P, Mahmoodian S, Stobbe S, Rauschenbeutel A, Schneeweiss P, Volz J, Pichler H and Zoller P 2017 *Nature* **541** 473
[13] Srivastava T, Chitriv S, Sahu S, Gorai P and Jha R 2022 *J. Appl. Phys.* **132** 203103
[14] Wu F, She Y C, Cheng Z M, Wu J J, Qi X, Wei Q, Xiao S Y, Sun Y, Jiang H T and Chen H 2023 *Physica B* **670** 415348
[15] Wu F, Liu T T, Long Y, Xiao S Y and Chen G Y 2023 *Phys. Rev. B* **107** 165428
[16] Zhang J, Zhou S, Dai X, Huang M and Yu X 2023 *Opt. Express* **31** 6062
[17] Cheng J, Xiang Y J, Xu J H, Liu S L and Dong P 2022 *IEEE Photon. J.* **22** 12754
[18] Kim M, Lee D, Kim Y and Rho J 2022 *Nanophotonics* **11** 4591
[19] Xie L G, Qiu X D, Luo L, Liu X, Li Z X, Zhang Z Y, Du J L and Wang D Q 2017 *Appl. Phys. Lett.* **111** 191106
[20] Lin S, Hong J A, Chen Z H, Chen Y and Zhou X X 2022 *Opt. Express* **30** 4096
[21] Chen S Z, Ling X H, Shu W X, Luo H L and Wen S C 2020 *Phys. Rev. Appl.* **13** 01405
[22] Sui J Y, Xu J, Liang A W, Zhou J H, Wu C Q, Zhang T H and Zhang H F 2023 *Sensors* **23** 4747
[23] Sui J Y, Zou J H, Liao S Y, Li B X and Zhang H F 2023 *Appl. Phys. Lett.* **122** 231105
[24] Morin F J 1959 *Phys. Rev. Lett.* **3** 34
[25] Zylbersztejn A and Mott N F 1975 *Phys. Rev. B* **11** 4383
[26] Li D S, Sharma A A, Gala D K, Shukla N, Paik H, Datta S, Schlom D G, Bain J A and Skowronski M 2016 *ACS Appl. Mater. Interfaces.* **8** 12908
[27] Currie M, Mastro M A and Wheeler V D 2017 *Opt. Mater. Express* **7** 1697
[28] Luo H L, Ling X H, Zhou X X, Shu W X, Wen S C and Fan D Y 2011 *Phys. Rev. A* **84** 033801
[29] Zhan T R, Shi X, Dai Y Y, Liu X H and Zi J 2013 *J. Phys.: Condens. Matter* **25** 215301
[30] Pan M M, Li Y, Ren J L, Wang B, Xiao Y F, Yang H and Gong Q H 2013 *Appl. Phys. Lett.* **103** 071106
[31] Yang W, Ang L K, Zhang W, Han J G and Xu Y 2023 *Opt. Express* **31** 27041
[32] Ahlawat L, Kishor K and Sinha R K 2024 *Opt. Laser Technol.* **170** 110183
[33] Singh R R, Kumari S, Gautam A and Priye G 2018 *IEEE. J. Sel. Top. Quantum Electron.* **25** 7300608
[34] Rakhshani M R 2019 *J. Opt. Soc. Am. B* **36** 2834
[35] Sani M H and Khosroabadi S 2020 *IEEE Sens. J.* **20** 7161
[36] Novais S, Ferreira C I A, Ferreira M S and Pinto J L 2018 *IEEE Photon. J.* **10** 6803609
[37] Natesan A, Govindasamy K P, Gopal T R, Dhasarathan V and Aly A H 2019 *IET Optoelectron.* **13** 117
[38] Askari A and Hosseini M V 2020 *J. Opt. Soc. Am. B* **13** 2712
[39] Anwar S and Khan M 2023 *Eur. Phys. J. E* **46** 19